Probabilistic 3D Mapping based on GNSS SNR Measurements

Andrew T. Irish, Jason T. Isaacs, François Quitin, João P. Hespanha, and Upamanyu Madhow

***Abstract*— A probabilistic approach to 3-dimensional mapping is proposed that only uses data gathered by GNSS (Global Navigation Satellite System) devices. To accomplish this, the environment is gridded and a physically motivated sensor model is developed that assigns likelihoods of blockage to satellite signals based on their measured SNR (signal-to-noise ratio). It is then shown that the posterior distribution of the map represents a sparse factor graph on which a low complexity implementation of Loopy Belief Propagation can be used for efficient Bayesian estimation. Experimental results are presented which demonstrate our algorithm's ability to coarsely map in three dimensions a corner of a university campus.**

I. Introduction

Reliance on Global Navigation Satellite Systems (GNSS), such as the Global Positioning System (GPS), has become ubiquitous with the advent of consumer electronics including smartphones. While principally serving as navigation aids, GNSS devices can also be viewed as *passive environment sensors,* as follows: 1) When a GNSS receiver traverses an area, obstacles such as buildings, trees, and terrain frequently block the line-of-sight (LOS) to various satellites, resulting in "shadowed", non line-of-sight (NLOS) channels characterized by statistically lower received signal strength; 2) The same receivers can record the data describing such shadowing events, including per-satellite azimuth, elevation and signal-to-noise ratio (SNR), along with the computed receiver coordinates. It can thus be argued that consumer GNSS devices represent a vast source of continuously updated mapping data.

Contributions: We provide and experimentally demonstrate a Bayesian algorithm for building probabilistic 3D maps using GNSS data as only source of measurements. Specifically, we show that by discretizing the environment and using a physically inspired nonlinear sensor model, the posterior distribution of the map represents a factor graph, on which an approximate mapping solution can be efficiently computed using Loopy Belief Propagation (LBP). We evaluate our algorithm on experimental data gathered using a handheld device.

Related work: Since GNSS accuracy degrades in cluttered urban environments, the dual problem to mapping – refining position estimates using *known* environment maps – is more well researched to date. A technique which has been used to achieve significant localization improvement is *Shadow Matching* (SM) [1]–[3]. Essentially, SM involves classifying signals as LOS/NLOS and matching their points of reception to areas outside/inside the "shadows" of signal-blocking buildings, thereby constraining the space of possible receiver locations. However, SM relies on up-to-date 3D maps which are not always available and can be expensive to obtain.

The problem of using GNSS signal strength to construct environment maps, as is our goal here, has received less attention. Currently published approaches [4], [5] learn shadows of buildings from GNSS information as in SM, and then employ non-probabilistic heuristics based on ray tracing to reconstruct environment maps. To the best of our knowledge, the present paper is the first to apply a systematic Bayesian approach to such shadow-based mapping. We believe that a probabilistic approach is more appropriate in general due to the large measurement uncertainty involved and the realization that empty space is more easily identified than occupied space.

Of course, Bayesian approaches are now standard in localization and mapping problems [6], with both the environment and sensor readings being modeled probabilistically. However, existing Bayesian algorithms are all based on implicit or explicit measurements of distances to obstacles, using a variety of sensing methods such as lidar/radar [7], [8], mono/stereo camera [9], [10], and WiFi [11]. Our sensing model is fundamentally different from these: an SNR measurement for a given satellite only gives us probabilistic information about whether or not the ray to the satellite is blocked, which makes the "data association problem" [6] of associating measurements with map features particularly challenging. To get around this, we represent the environment as an Occupancy Grid [12], a volumetric model that – while less common than feature-based representations – facilitates data correspondence by quantizing measurement rays, as illustrated in Figure 1. Unlike traditional Occupancy Grid mapping, however, we model the grid elements as strongly dependent using a factor graph [13], which captures the complex interactions between measurement rays that span (and thus intertwine) widely separated portions of the map.

In addition to the radically different measurement geometry, there is another key difference between our model and range-based Bayesian algorithms. Range sensors typically operate within a *local* reference frame, and thus provide readings that are sensitive to pose errors. In the GNSS mapping problem, *global* satellite/receiver coordinates (and hence the measurement beam directions) are known. As a

A.T. Irish, J.T. Isaacs, J.P. Hespanha and U. Madhow are with the Electrical and Computer Engineering Department, University of California, Santa Barbara (UCSB) ({andrewirish, jtisaacs, hespanha, madhow}@ece.ucsb.edu), F. Quitin is with the School of Electrical and Electronic Engineering, Nanyang Technological University, (fquitin@ntu.edu.sg)

This work was supported by the Institute for Collaborative Biotechnologies through grant W911NF-09-0001 from the U.S. Army Research Office. The content of the information does not necessarily reflect the position or the policy of the Government, and no official endorsement should be inferred.

978-1-4799-2893-4/14/$31.00 ©2014 IEEE

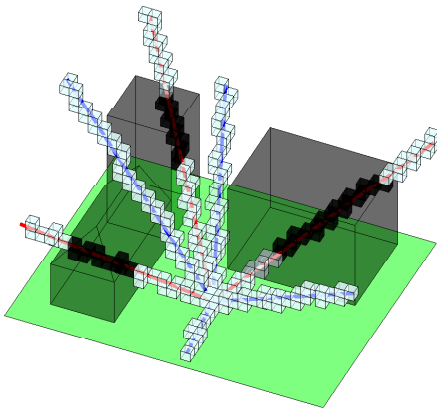

Fig. 1. Example occupancy grid illustration together with a SNR measurement scenario. Light/dark grid cells approximate empty/occupied space. Blue/red lines represent LOS/NLOS signal paths to satellites, with NLOS signals characterized by statistically lower SNRs.

result, the effects of positioning errors are partially "averaged out" by using large amounts of measurement data and by restricting ourselves to coarse grids (map resolutions). This allows for significant algorithmic simplifications; addressing the full simultaneous localization and mapping (SLAM) problem (see [14] for an introduction) is left for future work.

II. The Mapping Algorithm

A. Bayesian problem formulation

We represent the environment as an *Occupancy Grid*, a 3D grid of "map cells" $m = \{m_i\}_{i=1}^{L}$ with $m_i \in \{0,1\}$ denoting empty and occupied states respectively. The mapping problem is then formulated as estimating the occupancy probability of each cell m_i using information logged by GNSS receivers. The first piece of information is the set of *noisy* satellite SNR measurements, which consist of T vectors, $z = \{z_t\}_{t=1}^{T}$, where $z_t = [z_{t,1}, \ldots, z_{t,N_t}]$ contains individual SNR readings and N_t is the number of satellites in view at measurement index t. For every reading $z_{t,n}$ the receivers also provide satellite elevations and azimuths $[\theta_{t,n}, \phi_{t,n}]$, which we consider noiseless. The corresponding receiver position "fixes" are denoted $x = \{x_t\}_{t=1}^{T}$. As previously mentioned, in this paper we treat these as noiseless as well.

Under the "static world" assumption in which the environment is modeled as constant over time, the SNR measurements can be modeled as conditionally independent given the map and poses. Applying Bayes theorem to the posterior distribution of the map, we then have

$$p(m|x,z) = \frac{p(m)p(z|m,x)}{p(z)} \propto p(m)\prod_{t,n} p(z_{t,n}|x_t,m) \qquad (1)$$

where $p(m)$ is the prior distribution of the map. Although in this paper we assume the environment is completely unknown, the algorithm we develop in the upcoming sections also permits for map priors of the form $p(m) = \prod_i \psi_i(m_i)$.

B. SNR measurement model

The measured SNR of a given GNSS signal depends on a many factors in reality, including satellite elevation, environmental parameters, and receiver characteristics. While statistical models exist for the wireless channels of interest [15], [16], to avoid over-modeling and greatly simplify the LBP-based inference step, we define the measurement model as follows:

$$p(z_{t,n}|x_t,m) = \begin{cases} f_{LOS}(z_{t,n}), & m_i = 0 \ \forall \ i \in \mathscr{M}(t,n) \\ f_{NLOS}(z_{t,n}), & \text{otherwise} \end{cases} . \qquad (2)$$

In the above expression, f_{LOS} and f_{NLOS} are the Rice [17] and log-normal fading distributions, as illustrated in Figure 2, and $\mathscr{M}(t,n)$ indexes the map cells intersected by the ray starting at receiver position x_t in the direction of the transmitting satellite $[\theta_{t,n}, \phi_{t,n}]$. In other words, an SNR reading is LOS (Rice) distributed if *all* cells "observed" by its associated ray are empty; otherwise, it is NLOS (log-normal) distributed.

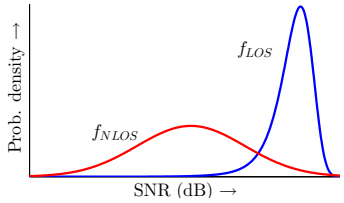

Fig. 2. The LOS/NLOS satellite channels are modeled according to Rician/log-normal distributions.

Physically, this approach assumes 1) that a LOS signal is well modeled as a superposition of a dominant LOS component and a circular Gaussian (multipath fading) component, and 2) a NLOS signal is subjected to random, multiplicative shadow fading. The setting of parameters, such as Ω, K for the Rice density, is discussed in Section III-A.

C. Inferring the map

The key realization of this paper is that the map posterior (1) describes a *factor graph* [13], a bipartite graph with variable nodes $\{m_i\}$ associated with the map state and factor nodes $\{f_{t,n}\}$ corresponding to the SNR likelihoods $\{p(z_{t,n}|x_t,m)\}$ (see Figure 3 for an illustration). Importantly, the graph is *sparse* due to the sensor model (2): each factor only depends on (is adjacent to) the relatively small set of map cells that are intersected by its associated ray. In addition, the factor graph contains cycles. A well-known technique that is used for efficient inference on such "loopy" factor graphs (and used in the context of mapping in [18]) is the *Loopy Belief Propagation (LBP)* [19], or *Sum-Product Algorithm* [13], an iterative message passing algorithm, which after convergence (assumed but not guaranteed) yields estimates of the variables' marginal posteriors.

1) Inference via reduced complexity LBP: As in standard LBP and shown in Figure 4, we have two types of messages passed locally in the factor graph. The message from variable m_i to an adjacent measurement factor $f_{t,n}$ is, for m_i defined on its domain $\{0,1\}$,

$$u_{i\to(t,n)}(m_i) \propto \psi_i(m_i) \prod_{(\tau,\eta)\in\mathscr{F}(i)\setminus(t,n)} U_{(\tau,\eta)\to i}(m_i) \, , \qquad (3)$$

where $\mathscr{F}(i)$ indexes the adjacent factors, $\psi_i(m_i)$ is the cell prior (uniform in this paper), and the messages are

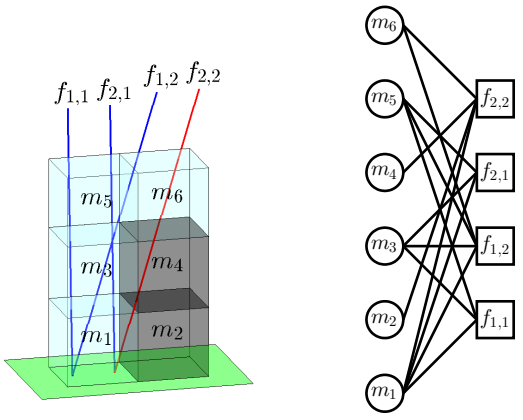

(a) Measurement scenario (b) Factor graph

Fig. 3. Simplified measurement scenario and its corresponding factor graph, with circles/squares representing variable/factor nodes. Note that map prior factors $\{\psi_i(m_i)\}$ are singly connected to their corresponding $\{m_i\}$ and are not shown for simplicity.

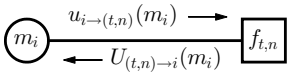

Fig. 4. Local message passing in Loopy BP and the notation used in this paper.

normalized to sum to one. In the other direction, employing the standard Sum-Product formula we have

$$U_{(t,n)\to i}(m_i) = \sum_{m\setminus m_i} p(z_{t,n}|m,x_t) \prod_{j\in\mathscr{M}(t,n)\setminus i} u_{j\to(t,n)}(m_j)\,, \quad (4)$$

where $\sum_{m\setminus m_i}$ is the marginalization sum over m_i, i.e., a sum over $2^{|\mathscr{M}(t,n)|-1}$ terms where $|\mathscr{M}(t,n)|$ in the number of cells observed by the SNR measurement. Because in our application measurement rays typically intersect tens of map cells, evaluating (4) directly is impractical. However, upon substitution of (2), we obtain the simple formula

$$U_{(t,n)\to i}(m_i) = \begin{cases} \gamma_{t,n,i}\cdot f_{LOS}(z_{t,n}) \;+ \\ \quad (1-\gamma_{t,n,i})\cdot f_{NLOS}(z_{t,n}) & m_i = 0 \\ f_{NLOS}(z_{t,n}), & m_i = 1 \end{cases} \quad (5)$$

where

$$\gamma_{t,n,i} = \prod_{j\in\mathscr{M}(t,n)\setminus i} u_{j\to(t,n)}(0)\,. \quad (6)$$

Thus, due to the LOS/NLOS measurement model, computing (4) has been reduced from exponential to linear complexity in the factor degrees.

After convergence of LBP, the marginal posterior of each map cell $p(m_i|x,z)$ is approximated by its "belief"

$$b_i(m_i) \propto \psi_i(m_i) \prod_{(t,n)\in\mathscr{F}(i)} U_{(t,n)\to i}(m_i) \quad (7)$$

which is normalized to sum to one. In this paper, we define convergence to be when the average of all belief residuals R_i falls below a predetermined threshold, where $R_i \triangleq |b_i^{new}(1) - b_i^{old}(1)|$.

III. Experiments and Results

Our 3D mapping algorithm was validated on GNSS measurement data taken outdoors from the eastern corner of the campus of the University of California, Santa Barbara (UCSB). The device used was a Samsung Galaxy Tablet 2.0 running on the Android operating system supporting both GPS and GLONASS. The overall data-set consisted of 14 streams of measurements taken over a few days, with each containing an average of 12 minutes of continuous measurement data arriving at 1 Hz. Reported satellite SNR readings ranged in the interval $7-48$ dB, and an average of 14 distinct satellites were in view at any point in time.

A. Parameter selection

A grid resolution of 4 m was selected and the map height was set to 24 m. For the LBP-based inference step, we used synchronous message passing [20] with a convergence threshold of 10^{-3}. To limit oscillations and aid convergence, 0.4 message damping was used (see [21] for a detailed explanation of damping). Referring to Section II-B, the total received power Ω under the LOS hypothesis was estimated as the maximum of all linear SNR readings $10^{z_{t,n}/10}$ from the same satellite during the same time window. For simplicity, we used a constant $K = 2$, indicating moderate fading conditions. Guided roughly by the results in [15], [22], the expected received power for NLOS links was set to 18 dB less than the "reference value" Ω, and the standard deviation was set to 10 dB, reflecting a large variability in shadowing conditions. Note that, although signals from low elevation satellites have wider power fluctuations [22], for simplicity the widths of both LOS/NLOS distributions were fixed across satellite elevations. However, for the same reason and much as in [4], a threshold satellite elevation of 10° was chosen, below which SNR measurements were discarded. When visibility to a particular satellite was temporarily lost in the middle of an observation window (presumably most often caused by total occlusion), the satellite coordinates were interpolated and LOS/NLOS likelihoods of 0.1/0.9 were used.

B. Discussion of results

Altogether, the 14 data-sets comprised of 1.4×10^5 SNR measurement rays and 4.6×10^4 map cells. However, the total execution time of our algorithm (ray tracing, graph indexing, LBP) was just under 5 minutes, carried out using MATLAB on a 64 bit PC with 4 GB of memory and a 2.40 GHz Intel Core i7-3517U processor.

A horizontal layer (4-8 m) of the resulting map – the *raw LBP output* – is compared to an aerial view of the same area in Figure 5. White and black areas correspond to estimated occupancy probabilities close to zero and one, respectively, with shades of grey denoting values in between. Blue cells are unexplored regions (those not intersected by any measurement rays). Green borders enclose the region in which measurements were taken, i.e., surround the feasible mapping region. The building contours, shown in red, were obtained from OpenStreetMap. Though the raw map slice

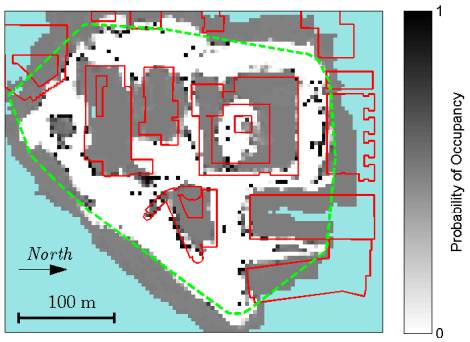

(a) Generated map

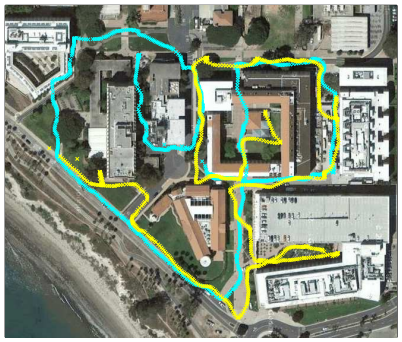

(b) Aerial view

Fig. 5. Horizontal slice (4-8 m above ground level) of generated map compared to Google Maps aerial view of the same area. In the aerial view, receiver paths from two typical datasets are shown.

in Figure 5 contains errors (some of which are possibly caused by receiver localization errors), approximate building locations and several large trees can be clearly identified.

Note that open areas are more easily (and *better*) mapped than occupied ones with our sensing model: while *every* cell a LOS signal passes through is empty, a NLOS signal only informs that *some* occupied cell(s) occluded it. Hence, if a NLOS ray spans many occupied cells, then each cell will have a tendency to "blame" (via message passing in LBP) other occupied ones for the blockage, contributing to uncertainty. Large obstacles can therefore be expected to result in "gray zones" with occupancy beliefs around 0.5, whereas empty space is more easily identified with high certainty. With this in mind, we expect that thresholding and/or image segmentation schemes applied to the output of the LBP algorithm may improve the map. While such post-processing strategies are beyond the scope of this paper, they are an important topic for future work.

The 3D mapping capability of our algorithm is demonstrated in Figure 6, showing the generated map around one building (Kohn Hall). Although the building in reality is about 10 m tall, the lingering region of cells above 12 m (red tinted cells) can be explained by the fact that only ground-level GNSS measurements were used, so that no LOS satellite signals glanced the middle part of the building roof (this is a limitation for any ray-based sensing method). Nevertheless, it can be concluded from the map data that Kohn Hall is no taller than 20 m, and for the most part shorter than 12 m. Separately, we note the empty (transparent) space surrounding the building that is correctly identified.

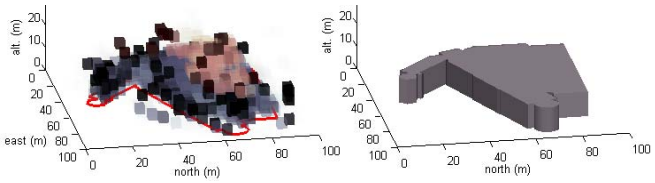

Fig. 6. Left: 3D occupancy map around Kohn Hall, with cell transparency set to emptiness probability (i.e., areas assigned low occupancy probabilities are transparent), and red tinted cells being those above 12 m. Right: approximate ground truth based on OSM data.

Finally, we explored the evolution of the map around another building, Harold Frank Hall, as more data becomes available in Figure 7. As expected, these results show that using a larger amount of measurement data improves the overall quality of the map and especially allows for better mapping of empty space.

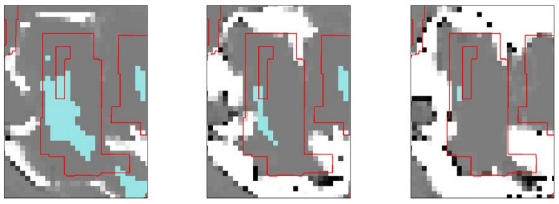

(a) 3 datasets (b) 7 datasets (c) 14 datasets

Fig. 7. Generated maps (4-8 m above ground level) around Harold Frank Hall as a function of the quantity of measurement data used.

IV. Conclusion and Future Work

We presented a probabilistic algorithm for mapping using GNSS SNR. The basic idea of our approach is to grid the environment, associate GNSS signals with likelihoods of being occluded, represent the map posterior as a factor graph, and employ LBP for efficient inference. We then validated our approach by coarsely mapping an outdoor area using a real-world dataset of GNSS SNR measurements.

The proposed approach constitutes a first step in a broader GNSS SNR based mapping and localization effort. As a next step, we aim to demonstrate the scalability of our approach by performing large scale mapping experiments and by using asynchronous LBP (and graph) update strategies. In addition, we seek to improve mapping and positioning accuracy through SLAM-like approaches, addressing the effects of receiver localization error via hybrid LBP/particle filtering methods.

Acknowledgement

The authors would like to thank Adam Ehrlich for developing the Android application used to record GNSS data.

REFERENCES

[1] L. Wang, P. D. Groves, and M. K. Ziebart, "Shadow matching: Improving smartphone GNSS positioning in urban environments," in *Proc. of the China Satellite Navigation Conference.*, 2013, pp. 613–621.

[2] B. Ben-Moshe, E. Elkin, H. Levi, and A. Weissman, "Improving accuracy of GNSS devices in urban canyons," in *Proc. of the 23rd Canadian Conference on Computational Geometry*, 2011.

[3] M. Obst, S. Bauer, P. Reisdorf, and G. Wanielik, "Multipath detection with 3D digital maps for robust multi-constellation GNSS/INS vehicle localization in urban areas," in *Proc. of the Intelligent Vehicles Symposium.*, 2012, pp. 184–190.

[4] K. Kim, J. Summet, T. Starner, D. Ashbrook, M. Kapade, and I. Essa, "Localization and 3D reconstruction of urban scenes using GPS," in *Proc. of the IEEE International Symposium on Wearable Computers.*, 2008, pp. 11–14.

[5] A. Weissman, B. Ben-Moshe, H. Levi, and R. Yozevitch, "2.5D mapping using GNSS signal analysis," in *Proc. of the Workshop on Positioning Navigation and Communication*, 2013, pp. 1–6.

[6] S. Thrun, "Robotic mapping: A survey," *Exploring Artificial Intelligence in the New Millennium*, vol. 1, pp. 1–35, 2003.

[7] S. Thrun, W. Burgard, and D. Fox, "A real-time algorithm for mobile robot mapping with applications to multi-robot and 3D mapping," in *Proc. of the International Conference on Robotics and Automation.*, vol. 1, 2000, pp. 321–328.

[8] M. W. M. G. Dissanayake, P. Newman, S. Clark, H. Durrant-Whyte, and M. Csorba, "A solution to the simultaneous localization and map building (SLAM) problem," *IEEE Trans. on Robotics and Automation*, vol. 17, no. 3, pp. 229–241, 2001.

[9] A. J. Davison, I. D. Reid, N. D. Molton, and O. Stasse, "MonoSLAM: Real-time single camera SLAM," *IEEE Trans. on Pattern Analysis and Machine Intelligence*, vol. 29, no. 6, pp. 1052–1067, 2007.

[10] P. Elinas, R. Sim, and J. J. Little, "σSLAM: Stereo vision SLAM using the Rao-Blackwellised particle filter and a novel mixture proposal distribution," in *Proc. of the International Conference on Robotics and Automation.*, 2006, pp. 1564–1570.

[11] B. Ferris, D. Fox, and N. Lawrence, "WiFi-SLAM using Gaussian process latent variable models," in *Proc. of the 20th International Joint Conference on Artificial Intelligence*, 2007, pp. 2480–2485.

[12] A. Elfes, "Occupancy grids: A stochastic spatial representation for active robot perception," in *Proc. of the Sixth Conference on Uncertainty in AI*, 1990.

[13] F. Kschischang, B. Frey, and H.-A. Loeliger, "Factor graphs and the sum-product algorithm," *IEEE Trans. on Information Theory*, vol. 47, no. 2, pp. 498–519, 2001.

[14] S. Thrun, "Simultaneous localization and mapping," in *Robotics and cognitive approaches to spatial mapping*. Springer, 2008, pp. 13–41.

[15] C. Loo, "A statistical model for a land mobile satellite link," *IEEE Trans. on Vehicular Technology*, vol. 34, no. 3, pp. 122–127, 1985.

[16] A. Abdi, W. C. Lau, M.-S. Alouini, and M. Kaveh, "A new simple model for land mobile satellite channels: first-and second-order statistics," *IEEE Trans. on Wireless Communications*, vol. 2, no. 3, pp. 519–528, 2003.

[17] A. Abdi, C. Tepedelenlioglu, M. Kaveh, and G. Giannakis, "On the estimation of the K parameter for the Rice fading distribution," *IEEE Communications Letters*, vol. 5, no. 3, pp. 92–94, 2001.

[18] A. Ranganathan, M. Kaess, and F. Dellaert, "Loopy SAM," in *Proc. of the International Joint Conference on Artificial Intelligence.*, 2007, pp. 6–12.

[19] J. Pearl, *Probabilistic Reasoning in Intelligent Systems: Networks of Plausble Inference*. Morgan Kaufmann Pub, 1988.

[20] G. Elidan, "Residual belief propagation: Informed scheduling for asynchronous message passing," in *Proc. of the 22nd Conference on Uncertainty in AI*, 2006.

[21] K. P. Murphy, Y. Weiss, and M. I. Jordan, "Loopy belief propagation for approximate inference: An empirical study," in *Proc. of the Fifteenth Conference on Uncertainty in Artificial Intelligence*, 1999, pp. 467–475.

[22] F. Perez-Fontan, M. Vazquez-Castro, S. Buonomo, J. P. Poiares-Baptista, and B. Arbesser-Rastburg, "S-band LMS propagation channel behaviour for different environments, degrees of shadowing and elevation angles," *IEEE Trans. on Broadcasting*, vol. 44, no. 1, pp. 40–76, 1998.